Showcasing research of López-Gallego's group: heterogeneous biocatalysis group at CIC biomaGUNE, San Sebastian-Donostia (Spain)

Cover design: A. L. Gallego (algtrespuntocero@gmail.com)

Selective biomineralization of $Co_3(PO_4)_2$-sponges triggered by His-tagged proteins: efficient heterogeneous biocatalysts for redox processes

His-tagged proteins drive the biomineralization forming sponge-like structures where both inorganic and biological elements co-localize. The bio-inorganic catalysts were re-used for several redox reaction cycles demonstrating their potential to be used in synthetic chemistry.

ROYAL SOCIETY OF CHEMISTRY

www.rsc.org/chemcomm

ChemComm

COMMUNICATION

Selective biomineralization of Co$_3$(PO$_4$)$_2$-sponges triggered by His-tagged proteins: efficient heterogeneous biocatalysts for redox processes†

Fernando López-Gallego*[ab] and Luis Yate[a]

We report a selective method to make functional bio-inorganic materials by mineralizing cobalt-phosphate in the presence of His-tagged enzymes. We have demonstrated that the His-tag drives the biomineralization forming sponge-like structures where both inorganic and biological elements co-localize. The bio-inorganic catalysts were re-used for several redox reaction cycles demonstrating their potential to be used in synthetic chemistry.

Recently, biomineralization has gained attention because the embedded proteins may present both higher stability and activity compared to their soluble counterparts.[1–4] The fabrication of biominerals does not require expensive pre-existing carriers because carrier synthesis and the protein immobilization occur simultaneously during the biomineralization. Interestingly, Zare's group discovered the fabrication of protein-embedded nanoflowers based on Cu$_3$(PO$_4$)$_2$·H$_2$O. This methodology has also been used to anchor multi-enzyme systems.[5,6] However, in spite of possessing such potential, this approach has not been tested to manufacture heterogeneous biocatalysts useful in synthetic chemistry. Hence, applications of these protein-hybrid nanoflowers have been limited to biosensing. On the other hand, the formation of the bio-inorganic nanoflowers relies on unspecific interaction of the protein with the Cu^{2+} ions.[2] Crucially, this feature makes the methodology universal but avoids controlling the orientation of the enzyme on the material surface. Opening this approach to selectively control both mineralization and orientation will contribute to expansion of its utility in other technological fields. Based on metal affinity chromatography, other less protein-reactive metals than copper, such as cobalt, should be able to selectively mineralize in the presence of His-tagged proteins, controlling the orientation of the proteins attached to the biominerals.[7,8]

Herein, we propose the synthesis of novel bio-inorganic structures, mineralizing Co$_3$(PO$_4$)$_2$ in the presence of enzymes tagged with the 6× His-tag. We hypothesize that such a His-tag will selectively drive the mineralization acting as a nucleation site for Co$_3$(PO$_4$)$_2$ nanocrystals that will further grow as bio-inorganic particles. To prove this hypothesis we have tested two Zn-dependent alcohol dehydrogenases extracted from *Geobacillus stearothermphilus*[10–12] (*his*Bs-ADH) and from *Lactococcus lactis* (*his*Ll-ADH), tagged with 6 histidines at their N-terminus. These enzymes are highly interesting in synthetic chemistry because they efficiently perform redox reaction under very mild conditions. Firstly, we incubated *his*Bs-ADH with CoCl$_2$ in the presence of phosphate saline buffer (PBS).

After three days we observed the formation of biominerals incorporating 50% of the offered protein and the immobilized *his*Bs-ADH presented 44% of the soluble specific activity (Table 1). Contrarily, untagged Bs-ADH incubated with PBS and CoCl$_2$ did not yield any active biomineral (Table 1). Moreover, His-tagged proteins were not attached to cobalt-phosphate particles spontaneously formed. These insights demonstrate that the His-tag is required to trigger the formation of Co$_3$(PO$_4$)$_2$ particles anchoring active enzymes.

Interestingly, Cu$_3$(PO$_4$)$_2$ biominerals presented similar immobilization yields but inactivated the oxidoreductase activity

Table 1 Biomineralization parameters

Enzyme	Mineral[a]	His-tag	Ψ[c] (%)	RsA[d] (%)
Bs-ADH	Cu$_3$(PO$_4$)$_2$	Yes	57 ± 2	1.74 ± 0.03
	Co$_3$(PO$_4$)$_2$	Yes	53 ± 2	44 ± 2
	Co$_3$(PO$_4$)$_2$	No[b]	19 ± 3	0.18 ± 0.13
Ll-ADH	Cu$_3$(PO$_4$)$_2$	Yes	96 ± 2	42 ± 3
	Co$_3$(PO$_4$)$_2$	Yes	97 ± 1	94 ± 2

[a] Mineralization was carried out with a PBS solution containing 0.1 mg mL^{-1} of enzyme and 0.8 mM divalent metal salt (CuSO$_4$ or CoCl$_2$). [b] The His-tag was removed from Bs-ADH by thrombin digestion. [c] Ψ (immobilization yield) = (protein concentration in the supernatant after 3 days of biomineralization/initial protein concentration before adding the metal salt) × 100. [d] RsA (%) (relative specific activity) = (sAbiomineral (U mg^{-1})/sAsoluble (U mg^{-1})) × 100.

[a] CIC biomaGUNE, Paseo Miramon 182, 20009, Donostia-San Sebastian, Spain.
  E-mail: flopez.ikerbasque@cicbiomagune.es
[b] IKERBASQUE, Basque Foundation for Science, Bilbao, Spain
† Electronic supplementary information (ESI) available: SEM, EDX, XPS analysis and some functional characterization data. See DOI: 10.1039/c5cc00318k

(Table 1 and Fig. S1, ESI†). Copper also has a similar but less dramatic effect on the activity of *hisLl-ADH* during the biomineralization process while cobalt enabled the *hisLl-ADH* biomineralization with negligible activity loss (Table 1). The higher enzyme activity recovered after the biomineralization of $Co_3(PO_4)_2$ instead of $Cu_3(PO_4)_2$ can be explained since soluble copper dramatically inactivated soluble Bs-ADH while soluble cobalt did not (Fig. S2, ESI†). This result suggests that copper unspecifically interacts with any protein domain causing the protein inactivation, whilst cobalt is extremely specific towards the His-tag and consequently does not affect protein stability. These two enzymes require two Zn^{2+} ions per subunit; one for activity, the other for stability.[13] In this scenario, copper, but not cobalt, may replace zinc, negatively affecting both activity and stability.[9,14] We suggest that copper replaces structural zinc instead of the catalytic one because the former is much more accessible to the bulk solution. In fact, other enzymes, like carbonic anhydrase, are not inactivated by biomineralization of $Cu_3(PO_4)_2$[2] because they only present the catalytic zinc buried into the active center.[2] Hence, cobalt seems to be a suitable metal to mineralize those enzymes containing structural divalent cations.

As we mentioned above, the His-tag is mandatory to efficiently mineralize proteins with cobalt-phosphate (Table 1). In fact, by using an *E.coli* crude over-expressing *hisBs-ADH*, only the protein containing the histidine-tag was selectively incorporated into cobalt-phosphate minerals among the untagged pool of proteins (Fig. S3, ESI†). This selective mineralization may rely on the low affinity of Co^{2+} for proteins lacking the His-tag, which explains that untagged proteins hardly induce the formation of $Co_3(PO_4)_2$ mineral particles.[7]

This result also reinforces the idea that cobalt does not bind to protein regions where either activity or stability might be negatively affected.

Based on both structural (SEM and EDX) and functional results we proposed a three-step mechanism for self-assembly of the bio-inorganic particles (Fig. 1A). Initially, the His-tag of *hisBs-ADH* binds Co^{2+} ions through coordination bonds. These specific metal protein complexes act as specific nucleation points to start the biomineralization of $Co_3(PO_4)_2$, forming 1 µm spheres (Fig. 1B). As a result, the enzyme molecules are efficiently attached to such spheres through their His-tags preserving their specific activity, likely because the enzymes are fairly exposed to the media, facilitating the diffusion of the substrates to the active sites (Fig. S4, ESI†). In a second stage, such spherical particles aggregate to form larger sponge-like particles (Fig. 1C). We suggest that during the aggregation of the small particles some particle-particle interactions displace a fraction of the outer protein layer, solubilising them into the media and thus lowering the immobilization yield. Simultaneously, another fraction of enzymes is buried by cobalt phosphate promoting either negative conformational changes or mass transfer limitations, both explaining the reduction of the global specific activity (Fig. S4, ESI†). Finally, the third stage involves the growth of cobalt phosphate over the sponge-like structures synthesized in step two, sculpting them into larger, more anisotropic and less packed forms (Fig. 1D). These particles show dramatically low enzyme specific activity likely because most of the enzymes are not accessible to the media, thus limiting their accessibility to the substrates (Fig. S4, ESI†). Furthermore, we also observed that the lower packing of these latter bio-inorganic
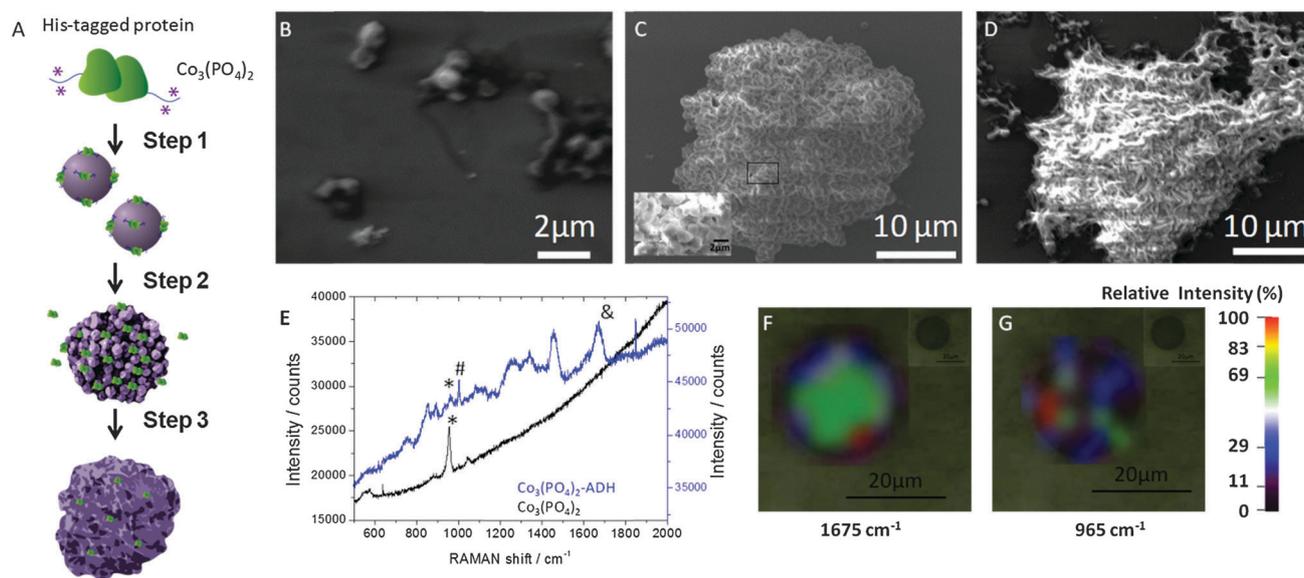
Fig. 1 Structural and physico-chemical characterization of Bs-ADH/$Co_3(PO_4)_2$ sponges. Proposed mechanism comprising three steps: (1) nucleation, (2) aggregation and (3) anisotropic growth (A). SEM images taken on 1 (B), 3 (C) and 12 (D) days. The inset of (C) corresponds to the 4.5× magnification of the region indicated by the black box. RAMAN spectra (E) of $Co_3(PO_4)_2$-biosponges (blue line) and control $Co_3(PO_4)_2$ precipitate (black line). Different characteristic RAMAN peaks were identified at 1675 cm⁻¹ for the amide I band (&) and at 1005 cm⁻¹ for Phe residues (#) of Bs-ADH and at 965 cm⁻¹ for the P−O stretching band of the $Co_3(PO_4)_2$ precipitate (*). RAMAN 2-D maps of Bs-ADH bio-inorganic sponges by monitoring signals at 1675 cm⁻¹ (F) and 965 cm⁻¹ (G). Maps were recorded at the equatorial plane of the particles by using a confocal RAMAN microscope.

sponges agrees with the higher hydration of the biomineral after 12 days ($Co_3(PO_4)_2 \cdot 8H_2O$, pink colour) compared to the bio-mineral after 3 days (anhydrous $Co_3(PO_4)_2$, violet colour) as was previously described[15] (Fig. S5, ESI†). The growth mechanism of these novel bio-inorganic sponges triggered by the His-cluster tagged to the enzyme seems to follow an amorphous aggregation of small nucleation sites that ensure the mineral growth. Hence, this mechanism is different from both the unspecific bio-mineralization of proteins with $Cu_3(PO_4)_2$[2] and the spontaneous formation of flower-like $Co_3(PO_4)_2$ particles.[16] Both mechanisms are based on the formation of crystalline nanoplates (or petals) starting from many different unspecific nucleation sites that further aggregate to form the larger particles.

RAMAN spectroscopy was employed to thoroughly character-ize the resulting bio-inorganic sponges. Fig. 1E shows RAMAN peaks at 1675 cm^{-1} and 1005 cm^{-1} corresponding to the amide I band and the Phe residues of the protein, respectively,[17] and at 965 cm^{-1} corresponding to P-O stretching of $Co_3(PO_4)_2$.[15] Furthermore, both 1675 cm^{-1} and 965 cm^{-1} signals co-localized across the biomineral particles, demonstrating the presence of the enzyme as part of the spongy structure, and observing a more uniform distribution of the protein than the phosphate (Fig. 1F and G). Atomic composition determined by EDX supported the RAMAN data (Fig. S6, ESI†). Noteworthily, neither RAMAN nor EDX analysis detected protein signals in control cobalt-phosphate crystals (Fig. S7, ESI†). Nevertheless, the low cobalt content on the surface of the bio-inorganic sponges grown for 3 days intrigued us (Fig. S6E, ESI†) because such an element was clearly present at the surface of control $Co_3(PO_4)_2$ crystals (Fig. S7D, ESI†). These data suggest that the proteins are distributed throughout the whole volume of the particles (Fig. S6H, ESI†) but mostly located at the most superficial layer of the bio-inorganic sponges. This suggestion was confirmed by analyzing the bio-inorganic sponges using XPS at different depths by etching the sample, confirming the presence of Co^{2+} (Fig. S8A, ESI†), and more interestingly that the deeper we measured, the higher cobalt and lower nitrogen contents were detected (Fig. S8B, ESI†). There-fore, XPS studies agree with both RAMAN and EDX analysis, confirming that the proteins are distributed throughout the whole volume of the 3-days particles but mostly located at the most superficial layer of the bio-inorganic sponges.

To aim at the optimal heterogeneous biocatalyst, we have selected the bio-inorganic sponges with optimal size to be easily recycled and with the highest catalytic activity. Based on such criteria, we have selected the bio-inorganic sponges grown for 3 days as suitable heterogeneous biocatalysts. We firstly bio-chemically characterized *his*Bs-ADH bio-inorganic sponges (Table S1, ESI,† Fig. 2). Kinetic parameters towards NADH were very similar for both soluble and mineralized *his*Bs-ADH, although the soluble enzyme presented 6-fold higher catalytic efficiency towards acetone than the biomineralized enzyme. This fact was mainly because of the higher K_M value towards acetone for the insoluble preparation (Table S1, ESI†).

In other hand, the optimal pH of the *his*Bs-ADH anchored to $Co_3(PO_4)_2$ sponges was 6 while the soluble enzyme presented an optimal value of 7 (Fig. 2A). The biomineralization made this

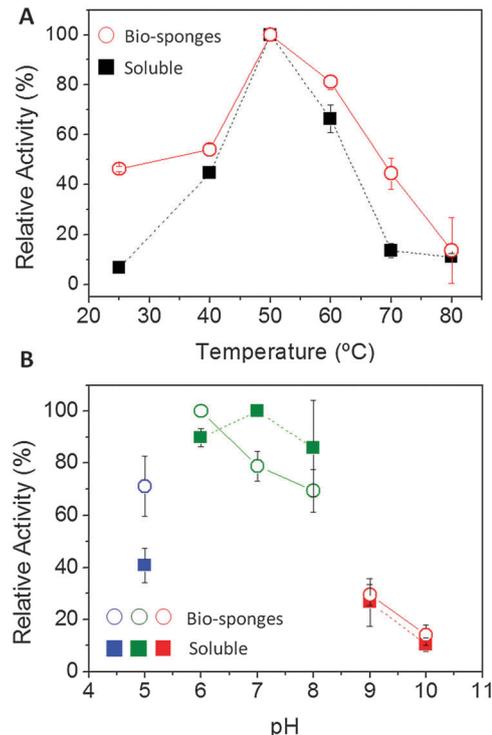Fig. 2 Biochemical characterization of Bs-ADH/$Co_3(PO_4)_2$ sponges. Activity–temperature profile (A) and activity–pH profile (B) of both soluble Bs-ADH (full squares, dashed line) and Bs-ADH bio-inorganic sponges (open circles, solid line). These data were calculated for the reduction activity towards acetone. For the activity–pH profile different buffers (blue-sodium acetate, green-sodium phosphate and red-sodium carbonate) were used.

enzyme more active under more acid conditions, overall at pH 5. The biomineral surface may be buffering the microenvironment of enzyme preserving neutral pH values at the enzyme vicinity even in acid media.[18] Furthermore, the optimum temperature for both soluble and mineralized enzymes was 50 °C although the activity of mineral preparation was less sensitive to the temperature than the soluble enzyme (Fig. 2B). The wider activity–temperature profile is supported by the higher stability of the mineralized *his*Bs-ADH that presented a half-life time at 70 °C of 45 minutes compared to 30 minutes presented by its soluble counterpart under the same conditions (Fig. S9, ESI†).

We have tested this heterogeneous biocatalyst in two different redox reactions that require nicotinamide redox cofactors. The heterogeneous enzyme was able to reduce acetone to isopropanol by using NADH as a cofactor which is further oxidized to NAD^+ (Fig. S10, ESI†). The same heterogeneous enzyme oxidized alcohols to aldehydes as well (Fig. S10, ESI†). The reduction reaction was irreversible and achieved 100% conversion of the redox cofactor, nevertheless the enzyme could only complete 30% of the oxidation reaction due to thermodynamic reasons; reduction of the product was catalytically more favourable than oxidation of the substrate. These redox reactions are very interesting to recycle oxidized (NAD^+) and reduced (NADH) nicotinamide cofactors by using acetone and ethanol as co-substrates, respectively. Both acetone and ethanol might also play a double role as a solvent and scarifying substrate for replenishing the suitable redox cofactor. We finally
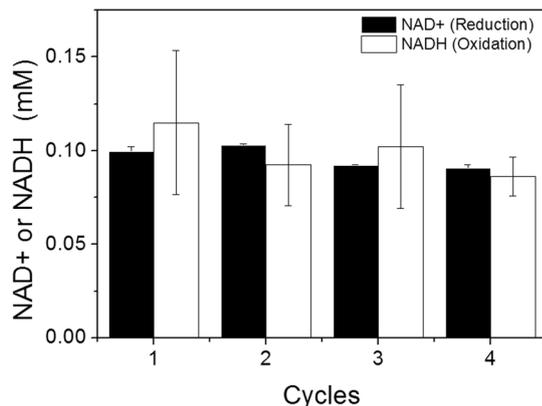
Fig. 3 Reusability of Bs-ADH bio-inorganic sponges. The recycling of the heterogenous biocatalyst was tested for two reactions; reduction of acetone (black bars) and oxidation of ethanol (white bars). The maximum yield after each reaction cycle was determined by measuring absorbance at 340 nm that indicated either the formation of NAD^+ by consumption of NADH (reduction reaction) or the formation of NADH (oxidation reaction).

tested the reusability of the *his*Bs-ADH optimally mineralized with $Co_3(PO_4)_2$ in several operational cycles for the abovementioned reactions. In both cases the heterogeneous catalyst was recycled up to 4 times with negligible activity loss (Fig. 3), which indicated that both recoverability and stability of the immobilized biocatalyst were efficiently achieved.

Hence, we can conclude that the biomineralization protocol of *his*Bs-ADH with $Co_3(PO_4)_2$ is revealed as an attractive methodology to immobilize enzymes without negatively affecting their kinetic properties but gaining stability and more importantly heterogeneity that allow this biocatalyst to be re-used in different chemical reactions.

We have reported an innovative selective method to make functional bio-inorganic materials by mineralizing cobalt-phosphate in the presence of His-tagged enzymes. These bio-inorganic sponges based on cobalt phosphate might be of great interest for heterogeneous biocatalysis of redox reactions. The copper phosphate minerals have been revealed to be deleterious for those enzymes containing structural divalent metals exposed at their surfaces, likely because copper ions can replace the structural

zinc cations, destabilizing the enzymes. In this work, we have found an alternative mineral to avoid such inactivation; cobalt-phosphate. Furthermore, the fabrication of functional biominerals may easily combine biological function with metal catalysis. For example, this type of bio-inorganic sponge opens new opportunities to combine biocatalysis and electrochemistry because of the high potential of cobalt-phosphate in water-splitting[19]. In the future, we envision these biominerals to carry out light-driven water splitting catalyzed by cobalt-phosphate, producing electrons as reducing power required by the mineralized redox enzymes to catalyze chemical reduction reactions.

Notes and references

1 L.-B. Wang, Y.-C. Wang, R. He, A. Zhuang, X. Wang, J. Zeng and J. Hou, *J. Am. Chem. Soc.*, 2013, **135**, 1272–1275.
2 J. Ge, J. Lei and R. N. Zare, *Nat. Nanotechnol.*, 2012, **7**, 428–432.
3 H. Cao, D.-P. Yang, D. Ye, X. Zhang, X. Fang, S. Zhang, B. Liu and J. Kong, *Biosens. Bioelectron.*, 2015, **63**, 329–335.
4 C. L. Henriquez, I. Junior, R. O. M. a de Souza and R. Luque, *Catal. Sci. Technol.*, 2014, DOI: 10.1039/C4CY01313A.
5 Z. Li, Y. Zhang, Y. Su, P. Ouyang, J. Ge and Z. Liu, *Chem. Commun.*, 2014, **50**, 12465–12468.
6 J. Sun, J. Ge, W. Liu, M. Lan, H. Zhang, P. Wang, Y. Wang and Z. Niu, *Nanoscale*, 2014, **6**, 255–262.
7 E. Sulkowski, *BioEssays*, 1989, **10**, 170–175.
8 L. Andersson and E. Sulkowski, *J. Chromatogr. A*, 1992, **604**, 13–17.
9 R. Karlstrom and R. L. Levine, *Proc. Natl. Acad. Sci. U. S. A.*, 2000, **88**, 5552–5556.
10 C. Ceccarelli, Z.-X. Liang, M. Strickler, G. Prehna, B. M. Goldstein, J. P. Klinman and B. J. Bahnson, *Biochemistry*, 2004, **43**, 5266–5277.
11 R. Cannio, M. Rossi and S. Bartollucci, *Eur. J. Biochem.*, 1994, **222**, 345–352.
12 G. Fiorentino, R. Cannio, M. Rossi and S. Bartolucci, *Protein Eng.*, 1998, **11**, 925–930.
13 D. S. Auld and T. Bergman, *Cell. Mol. Life Sci.*, 2008, **65**, 3964–3970.
14 J. H. R. Klgi and B. L. Vallee, *J. Biol. Chem.*, 1960, **235**, 3188–3193.
15 T. Karam, H. El-Rassy, F. Zaknoun, Z. Moussa and R. Sultan, *Chem. Phys. Lett.*, 2012, **525–526**, 54–59.
16 M. Badsar and M. Edrissi, *Mater. Res. Bull.*, 2010, **45**, 1080–1084.
17 R. Tuma, *J. Raman Spectrosc.*, 2005, **36**, 307–319.
18 R. C. Rodrigues, C. Ortiz, Á. Berenguer-Murcia, R. Torres and R. Fernández-Lafuente, *Chem. Soc. Rev.*, 2013, **42**, 6290–6307.
19 M. W. Kanan, Y. Surendranath and D. G. Nocera, *Chem. Soc. Rev.*, 2009, **38**, 109–114.